AIAA AVIATION Forum
August 2-6, 2021, VIRTUAL EVENT
AIAA AVIATION 2021 FORUM

10.2514/6.2021-2809

Check for updates

Investigation of flow-structure coupling for a compliant panel under a shock/boundary-layer interaction using fast-response PSP

Mustafa N. Musta[1], Yoo Jin Ahn[2], Marc A. Eitner[3], Jayant Sirohi[4], and Noel T. Clemens[5]
Department of Aerospace Engineering and Engineering Mechanics, The University of Texas at Austin, Austin, TX, 78712, USA

This experimental study aims to investigate and compare unsteady surface pressure fluctuations on rigid and compliant panels under a shock-wave/boundary-layer interaction (SBLI) generated by a 20° compression ramp in a Mach 2 wind tunnel. The compliant panel was made of 1mm thick polycarbonate and had a first mode resonant frequency of 407 Hz. High-speed simultaneous pressure-sensitive paint (PSP) and digital image correlation (DIC) techniques allow for examination of the panel surface pressure and panel displacement, respectively, with acquisition frequencies of 20 kHz and 5 kHz respectively. The PSP measurements were also made on the face of the rigid compression ramp and so the effect of fluid-structure interaction on the reattachment dynamics could be explored. The rigid panel pressure measurements demonstrated the spectral content inherent to the SBLI. Spectral analysis of the surface pressure fields revealed that the SBLI shock foot and separation shear layer behave as low- and high-frequency filters, respectively, and the compliant panel showed the similar behavior with the peak frequency at the first mode frequency of the panel (~407Hz). The spectral comparison of pressure fields also depicted that the other modes of the structural panel affected the flow (at frequency 624 Hz) near the compliant panel's mid-region. The results indicate the panel dynamics have a strong effect on separation- and reattachment-flow dynamics. Modes obtained by spectral proper orthogonal decomposition (SPOD) show good agreement with modes obtained from bandpass filtered displacement and pressure fields.

Downloaded by Noel Clemens on August 8, 2021 | http://arc.aiaa.org | DOI: 10.2514/6.2021-2809

δ_{99}	=	Boundary layer velocity height based on 99% free stream.
δ^*	=	Boundary layer displacement thickness
θ	=	Boundary layer momentum thickness
H	=	Boundary layer shape factor
U_{BL}	=	Boundary-layer edge velocity
U_∞	=	Freestream velocity
Re	=	Reynolds number
x	=	Streamwise coordinate
y	=	Wall-normal coordinate

I. Introduction

[1] Lecturer, Member
[2] Graduate Student, Member
[3] Graduate Student, Member
[4] Professor, Associate Fellow
[5] Professor, Fellow

Copyright © 2021 by the American Institute of Aeronautics and Astronautics, Inc. All rights reserved.

FLUID structure interactions (FSIs) are a challenging phenomenon that are often associated with hypersonic vehicles near control surfaces and engine inlets/isolators where strong unsteady pressure loading is present. An FSI can result in a strong and dynamic coupling between lightweight structural members of the vehicle and the flow, which can lead to structural fatigue or even failure of the compliant structures [1]. Further, in hypersonic flight, aerothermoelastic effects become problematic due to the heating resulting from viscous dissipation in the boundary layers. As a consequence of the heating, structural panels tend to become more compliant at higher Mach numbers if no active cooling is used. Therefore, the weaker structures associated with supersonic aircraft are particularly susceptible to the forcing by the strong pressure fluctuations associated with turbulent boundary layers and shock/boundary-layer interactions (SBLIs).

SBLIs are also ubiquitous on high-speed vehicles, commonly occurring on control surfaces, inlets, and turbine blades. SBLIs possess a broadband unsteadiness that is typically 10 to 100 times lower than the characteristic boundary layer frequency [2],[3] ($0.01< S_t< 0.10$). Even on non-compliant surfaces, SBLIs are associated with large oscillatory pressure and heat transfer loading [4]. Often the SBLI unsteadiness contains significant spectral content at, or near, resonant modes of the structural members on which they reside. Hence, the large oscillatory forcing close to resonant modes of structural members and heating makes SBLIs particularly prone to generating FSIs.

A number of different studies examine FSIs resulting from SBLIs occurring due to reflected shocks. Some studies have found that the mean loading on a thin structure affects the flow dynamics [5], and the FSI affects the shock foot frequency [6]. Recent studies by Spottswood et al. [7]–[9] demonstrate coupling at lower frequencies between panel displacement and surface pressure fields. Previous FSI works in the facility used in the current work have also examined the coupling present in a fluid-structure interaction generated by a 2D compression ramp over a compliant panel by simultaneous high-speed DIC and PSP measurements [10]–[13][14]. Shock foot motion locking to the first mode of the panel at lower frequencies together with the upstream and separation regions effects were observed.

This study examines the effects of coupling between a compliant panel under a Mach 2 compression ramp SBLI. The panel is made of polycarbonate and is 1 mm thick, and the primary diagnostics are DIC and PSP. PSP measurements are also made on the face of the ramp to enable investigation of the effect of FSI on SBLI reattachment dynamics. Further analysis was made for the compliant panel by using spectral proper orthogonal decomposition (SPOD) and bandpass filtering techniques applied to the DIC and PSP data. PSP measurements on the rigid panel were also made for comparison purposes. Pointwise spectral analysis was made on both compliant and rigid panels to evaluate the effect of panel flexibility.

A. Facility and Set-Up

The experiments were performed in the Mach 2 blow-down wind tunnel facility at The University of Texas at Austin, which provides a free stream velocity of 495 ms^{-1}, stagnation conditions of 261±7 kPa and 292±5 K, and a nominal run time of 30 seconds. The freestream turbulence intensity is less than 1%, and the freestream and wall condition unit Reynolds numbers are $Re_\infty=3.8\times10^7$ m^{-1} and $Re_w=4.67\times10^5$ m^{-1}, respectively. The test section boundary-layer thickness (δ_{99}) at the boundary layer edge velocity ($0.99U_\infty$) is 11.75 mm. The compressible momentum (θ) and displacement (δ^*) thicknesses are 0.9 mm and 2.6 mm, respectively, and Re_θ= 34,200 [15]. Further details of the test conditions can be found in previous studies [16], [17].

Downloaded by Noel Clemens on August 8, 2021 | http://arc.aiaa.org | DOI: 10.2514/6.2021-2809

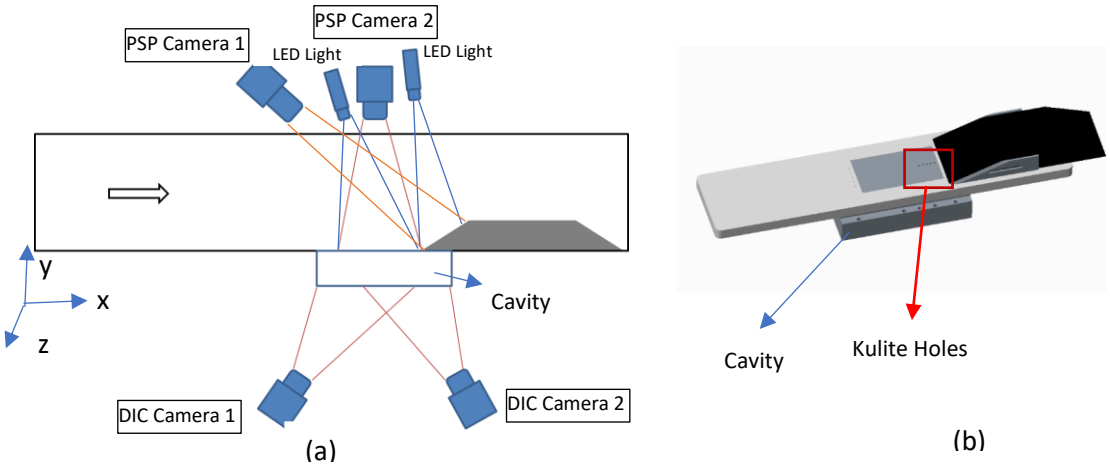

Figure 1. Experimental setup. (a) schematic for simultaneous PSP and DIC; (b) schematic of compression ramp with the rigid panel, tunnel floor, and cavity.

This study examines a 20° compression ramp as shown in Figure 1. The compression ramp was spanwise-centered in the wind tunnel with fences that extend 10 mm upstream of the ramp to prevent spillage and interaction with the corner vortices. A floor plug section facilitates installation of either a rigid panel or a thin compliant panel immediately upstream of the ramp-floor junction. A sealed window cavity was fitted below the compliant panel to allow arbitrary selection of the panel backpressure via an attached vacuum pump. However, it aimed to match the tunnel freestream static pressure, which is about 7 psi. For this experiment, the cavity pressure was set to 6.4 ± 0.1psi, which is slightly less than the freestream value. It was very difficult to match the exact freestream pressure because leaks between the cavity and test section necessitated that the vacuum pump be left on during the run. Essentially, it was a trial-and-error process to set the cavity pressure. The slightly low cavity pressure did cause a mean deflection of the compliant panel.

The windowed cavity allows an unobstructed view of the back surface of the compliant panel for digital image correlation (DIC). The compliant panel was made from polycarbonate, and was 127 mm long by 68.5 mm wide by 1 mm thick. The material and thickness of the compliant panel were selected to give the desired set of low modal frequencies of 351 Hz, 473 Hz, and 675 Hz that were calculated using analytical relations from Blevins & Plunkett [18]. More accurate modal frequencies were obtained by conducting impact-hammer testing of the installed panel. The first and second mode frequencies were measured to be 407 Hz and 542 Hz, respectively [23].

B. High-Speed Surface Pressure Measurements

To supplement the PSP measurements, high-frequency-response Kulite pressure transducers were used at discrete locations that depended on whether the rigid or compliant panels were being tested. The pressure transducers used in this study are ultra-miniature Kulite transducers (XCQ-062-50) and have a temporal response of approximately 50 kHz, as given by the manufacturer. The Kulite transducer measurements were made to provide: (*i*) *in situ* calibration of the PSP, (*ii*) assessment of the PSP dynamic response, and (*iii*) high-quality discrete surface pressure measurements for analysis. The rigid panel features five streamwise pressure transducer locations with a 3 mm pitch along the midline of the tunnel near the ramp junction (Figure 2a). These transducers are placed throughout the interaction region and so are good for both calibrating and assessing the temporal response of the PSP. The compliant panel features the same spanwise pressure transducer locations just upstream of the panel within the freestream, but no downstream transducers. These upstream transducers are used to provide an in-situ calibration of the PSP. The pressure transducers were calibrated at least once per day. A data acquisition system (National Instruments NIMax PXIe 1030) with two PXIe-4331 modules recorded the pressures from the transducers at 140 kHz and filtered the signal to 100 kHz. The total uncertainty of the pressure measurements is about 2% of the wall static pressure (~700 Pa), assessed by summing the component uncertainties according to a root-sum-of-squares law [19].

Downloaded by Noel Clemens on August 8, 2021 | http://arc.aiaa.org | DOI: 10.2514/6.2021-2809

C. High-Speed Pressure Sensitive Paint

The polymer/ceramic pressure-sensitive paint (PC-PSP) was considered for high-speed pressure measurements. The PSP uses a ruthenium luminophore ((Ru)ddp3), a silicon rubber binder, TiO2 base, and toluene solvent with a recipe of (Ru)ddp3 (15mg) + TiO2 (92%wt) + Silicone (8%wt) +Toluene(15ml) [20]. PSP images were recorded at 20 kHz using FastCam Mini and Nova S with two in house-made LED light sources (Figure 1a). The total number of images acquired per experiment is 32000, which was dictated by the camera memory. The panel was imaged fully with resolution 352 by 624 pixels (PSP Camera 1 in Figure 1a), and on the ramp over 66 mm by 66 mm area, it was acquired by 512 by 512 pixels. The light source emits at 450 ± 10 nm. The camera is fitted with a 550 nm long-wavelength-pass filter.

D. High-Speed Digital Image Correlation

Stereoscopic digital image correlation (DIC) allows measurement of the 3D surface deformation of the compliant panel. The DIC system uses two high-speed cameras (labeled DIC Camera 1 and 2 in Figure 1) to obtain full three-dimensional displacement fields of the panel surface. The DIC cameras (Phantom Miro M310) are mounted under the tunnel and acquired data at a frame rate of 5 kHz, with a total of 10,000 images per camera acquired over 2 seconds. A random speckle pattern is applied to the back of the compliant panel, which the system views from under the tunnel through the windowed cavity. All DIC images have been processed using LaVision DaVis v10 by setting an interrogation window size of 19x19 pixels with a 7-pixel overlap.

II. Results and Discussion

Previous studies made in this facility have examined SBLIs using simultaneous high-speed (6.4kHz-50kHz) PSP and stereo-DIC [11], [12], [14], [21], [13]. Trends are found in both data sets that are relevant to this study interms first mode effects on the flow and shock-foot first mode coupling etc. Compared to previous studies, the present study uses higher resolution PSP (20kHz) as well as 5kHz DIC measurements.

E. PSP Paint Calibration and Validation

The PSP paint calibration was calculated in-situ using the pressure transducers discussed earlier in section B. The calibration is achieved by comparing the run-averaged Kulite transducer measurements to run-averaged 'virtual transducers' that are extracted from the PSP. Figure 2(a) shows the mean pressure field, and the Kulite pressure transducer locations are shown as the line of circles near the ramp edge. A virtual transducer is a region of the PSP paint averaged over an area equivalent to the size of the Kulite transducers but displaced by 30 pixels. The static calibration can then be used to examine the dynamic response of the PSP and transducer measurements to validate the accuracy of the PSP. Figure 2(b) shows the spectral response for a pressure transducer nearest the ramp junction and the virtual transducer spanwise adjacent to it; this location was selected as the shear-layer has a significant high-frequency content which allows the response of the PSP to be better assessed. In Figure 2(b), we see that the spectral comparison between the PSP and the transducer is excellent, with the PSP following the transducer until the 10 kHz Nyquist limit is reached. However, it is noted that some of the very high-frequency content in the virtual transducer does appear to decline from the Kulite. Hence, the response of the PSP is appropriate for analysis of pressure fluctuations that are at a frequency (<8 kHz) liable to have been caused by or coupled to the panel.

Downloaded by Noel Clemens on August 8, 2021 | http://arc.aiaa.org | DOI: 10.2514/6.2021-2809

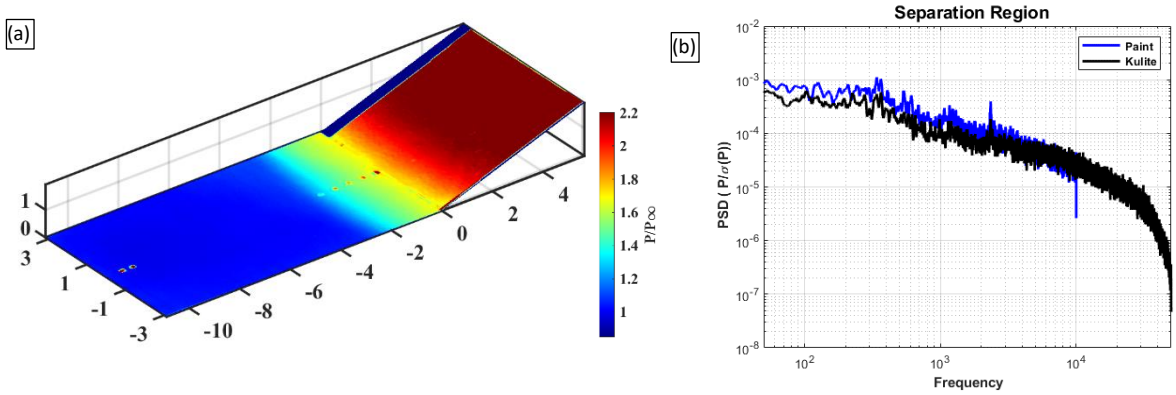

Figure 2. Comparison of rigid-panel PSP data vs. Kulite pressure transducer data. (a) Mean Pressure Field and (b) PSD of pressure from Kulite and virtual transducer near the same location.

F. Time Sequence of Pressure and Displacement Measurements

A time sequence of the displacement (y-direction) and pressure data is shown in Figure 3. Each row shows the same time instant for both images, and the time interval between rows is 0.40 ms. In the colormap used, the orange regions represent small out-of-plane displacement, whereas regions of large out-of-plane displacement are shown in blue. Notice that maximum displacement is biased toward the downstream end of the ramp, owing to the presence of the SBLI, which covers approximately the downstream 20% of the panel. The high-pressure region associated with the SBLI forces the compliant panel downwards at this location. For the pressure colormap, the blue is the free stream value, the aqua/green is the shock foot, the yellow/orange is the separation region, and the red is the high-pressure region on the ramp face. The black line represents the instantaneous surrogate shock foot location which was defined by a pressure isobar of P/P_∞=1.2. The time variation in both the pressure and displacement fields are clearly evident from Figure 3 (a-d). Between $x/\delta_{99} = -10$ and -2 we see that the panel is deflected downwards, which should be associated with a weak expansion of the flow and thus a decreasing pressure. Although not obvious from the colormap, such a decrease in pressure with downstream distance can be observed as a change from blue to dark blue. Movies generated from the images exhibit noticeable quasi-periodic pressure variation along with streamwise streak structures that are more random in character. Additionally, long turbulent structures moving from the surrogate shock foot to separation were observed, which could be the footprint of Görtler vortices that are known to form as a result of the streamline curvature associated with separation [4].

The correlation between the displacement and pressure field was analyzed using the cross-correlation algorithm using Matlab' xcorr' function. The cross-correlation was made initially between the displacement of an individual point on the panel and pressure at every point. The purpose of this analysis is to explore the relationship between motion of the panel and the global flow-field. Two displacement points were used that were on the spanwise centerline at downstream locations of $x/\delta_{99} = -5.2$ and -9. To get the entire field correlation coefficient, a pointwise cross-correlation was applied to the entire panel surface and the ramp excluding edges in the ($z/\delta_{99} = -2$ to 2). Figure 4 shows the peak correlation between the two displacement points at $x/\delta_{99} = -5.2$ and -9 (Figure 4a-b) and the pressure field. Casual examination of Figure 4 shows that there are two regions of high correlation on the panel, which are seen as the two broad red regions near $x/\delta_{99} \approx -8$ to -10 and $x/\delta_{99} \approx -4$ to -6**.** These two regions of high correlation show that there is a high level of flow coupling in those regions. This correlation has been explored in previous studies and is a result of response of the isentropic outer flow to the streamline curvature induced by first-mode vibration of the panel.

The correlation coefficient is small near the intermittent region, which is the region of shock-foot oscillation at about $x/\delta_{99} \sim -2.2$. The lack of correlation in this region is likely due to the effect of turbulence on the shock-foot motion. The correlation coefficient is about 0.4 near the separation line and even lower values on the ramp face. Despite the lower correlation values on the ramp face it will be shown below that the pressure on the ramp face is clearly tied to the oscillation cycle of the first panel mode.

Downloaded by Noel Clemens on August 8, 2021 | http://arc.aiaa.org | DOI: 10.2514/6.2021-2809

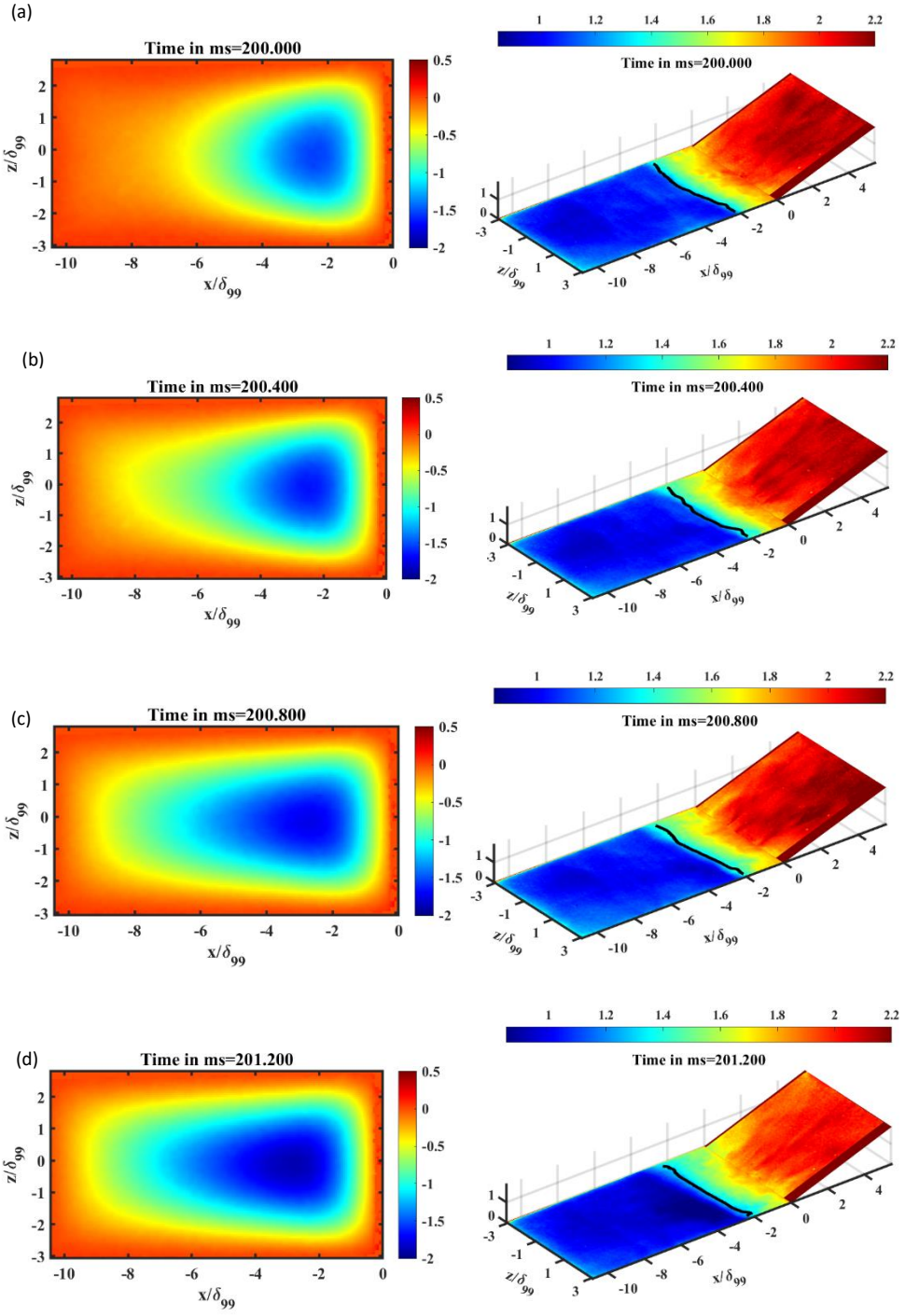

Figure 3. A time sequence of the displacement (left column) and pressure (right column). Instantaneous surrogate shock foot locations are represented on the pressure measurements in black color.

Downloaded by Noel Clemens on August 8, 2021 | http://arc.aiaa.org | DOI: 10.2514/6.2021-2809

Downloaded by Noel Clemens on August 8, 2021 | http://arc.aiaa.org | DOI: 10.2514/6.2021-2809

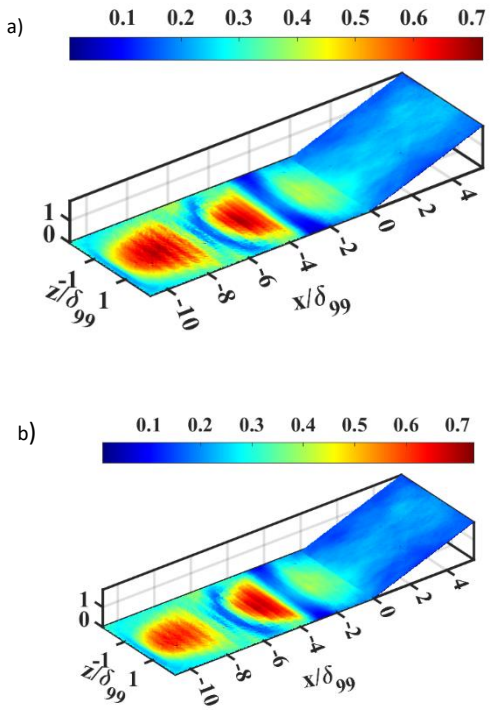

Figure 4. Cross-correlation coefficient between displacement points at $x/\delta_{99} = -5.2$ and -9.0 to the pressure field: a) x/δ_{99} = -5.2, b) x/δ_{99} = -9.0

G. Spectral Analysis

Virtual pressure transducers were examined at discrete locations to compare pressure fluctuations over the rigid panel to those of the compliant panel. The streamwise locations of $x/\delta_{99} = -0.8, -2.5$ and –10.3 (at the spanwise centerline), were used and corresponded to the separation region, the intermittent region, and the undisturbed inflowing boundary layer (respectively). Additionally, three locations were considered on the ramp face: x/δ_{99}=0.5, 2/3, and 4.4. The time histories of each virtual transducer were used to calculate pre-multiplied power spectral densities (PSD), which are shown in figures 5 and 6. Figure 7 compares power spectra of the displacement and virtual pressure signals at the locations: x/δ_{99}=-1.3, 5.3, and 10.3.

Figure 5 shows the surface pressure spectral content for the rigid and compliant panels at the inflow boundary layer ($x/\delta_{99} \approx -10.3$), near the intermittent region ($x/\delta_{99} \approx -2.5$), and within the separation region ($x/\delta_{99} \approx -0.5$). For all compliant cases, a significant peak is present at $f \approx 390$ Hz, which corresponds to the first mode vibrational frequency of the panel. All of the spectra exhibit a sharp peak at 2350 Hz, which appears to be present in the upstream boundary layer and its origin is not known. It may be some type of acoustic instability in the plenum section of the wind tunnel. Figure 5a shows the spectral content underneath the separated flow; it exhibits high-frequency content for both panels, which is an observation that is well known from the literature as being caused by pressure fluctuations from the separated shear layer; however, the compliant case also exhibits the strong first vibrational mode peak near 400 Hz. Figure 5b shows the spectral content for each panel under the intermittent region ($x/\delta_{99} \approx -2.5$), which is expected to be dominated by shock-foot motions that are known to be relatively low frequency (< 2 kHz). Indeed, both the rigid and compliant panels exhibit broadband low-frequency pressure fluctuations of nearly the same power spectral density; however, the compliant panel exhibits the strong first-mode peak near 400 Hz. Figure 5c shows the spectral content underneath the upstream boundary layer for which the power

spectral densities are quite low as compared to farther downstream. The first-mode peak is quite prominent at this station, which shows strong pressure-field coupling effectively starts from the upstream edge of the panel.

Figure 6 shows the surface pressure pre-multiplied PSDs on the ramp face for the rigid and compliant panels. Spectra are shown for the following locations: $x/\delta_{99} \approx 0.5, 2.3,$ and 4.4. We emphasize that the ramp is not compliant and so any pressure fluctuations at the panel vibratory frequencies were convected downstream with the flow. Indeed, Figure 6 shows that the 390 Hz first mode is relatively prominent at $x/\delta_{99} \approx 0.5$, but gets progressively weaker with increasing downstream distance. This suggests that the reattaching shear layer is likely to be coupled to the compliant panel dynamics.

Figure 7 compares the spectral content of displacement and virtual-pressure fluctuations. Downstream locations of $x/\delta_{99} \approx -1.4, -5.3,$ and -10.3 were considered. Figure 7a shows the comparison in the separation region. The displacement fluctuations show the presence of five peaks at 400 Hz, 625 Hz, 975 Hz, 1380 Hz, and 1915 Hz. Recall that the hammer impact test gave first and second mode frequencies of 407 Hz and 542 Hz. The first mode is in good agreement but the second mode less so. Previous work has documented that stiffening of the panel in the wind tunnel can occur due to both the pressure differential across the panel as well as aerodynamic cooling of the panel caused by the decrease in the stagnation temperature of the freestream flow with time [23]. In Figure 7b-c, the same level of agreement can be observed. In Figure 8b, it is interesting that the pressure spectrum shows the second-mode peak at 625Hz, but the corresponding displacement spectrum does not. The reason for this is likely because the $x/\delta_{99} \approx -5.3$ location is near a node for the second mode. The fact that a second-mode peak is observed in the pressure is because under the linear-flow assumption, the pressure is related to the local flow angle, and the flow angle varies significantly at the second-mode node. In Figure 7c, the displacement spectrum shows more modes, which indicates this point is not near a node.

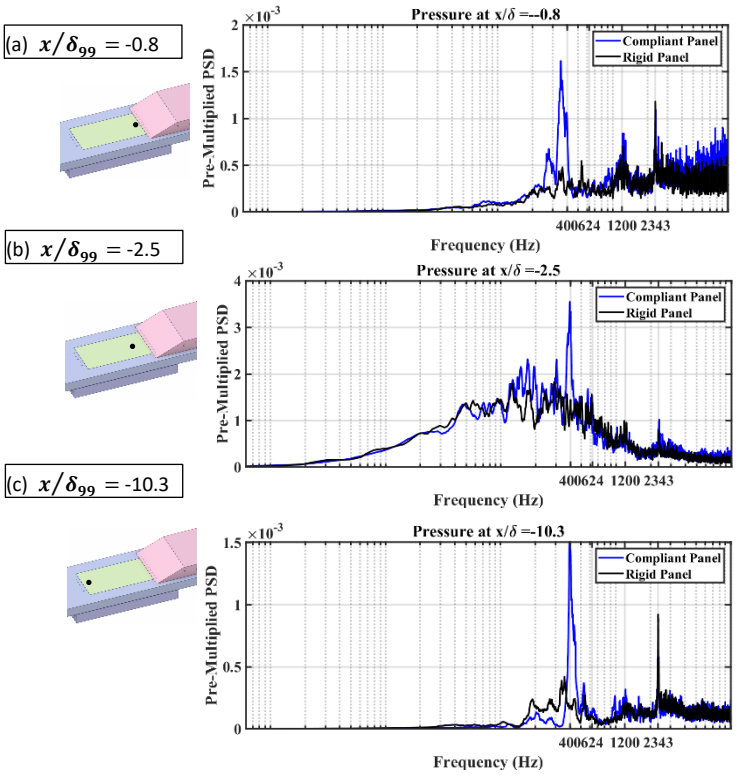

Figure 5. Pre-multiplied power spectra of virtual pressure transducer data for rigid and compliant panels. (a) x/δ_{99} = -0.8, (b) x/δ_{99} = -2.5, and (c) $x/\delta_{99} = -10.3$

Downloaded by Noel Clemens on August 8, 2021 | http://arc.aiaa.org | DOI: 10.2514/6.2021-2809

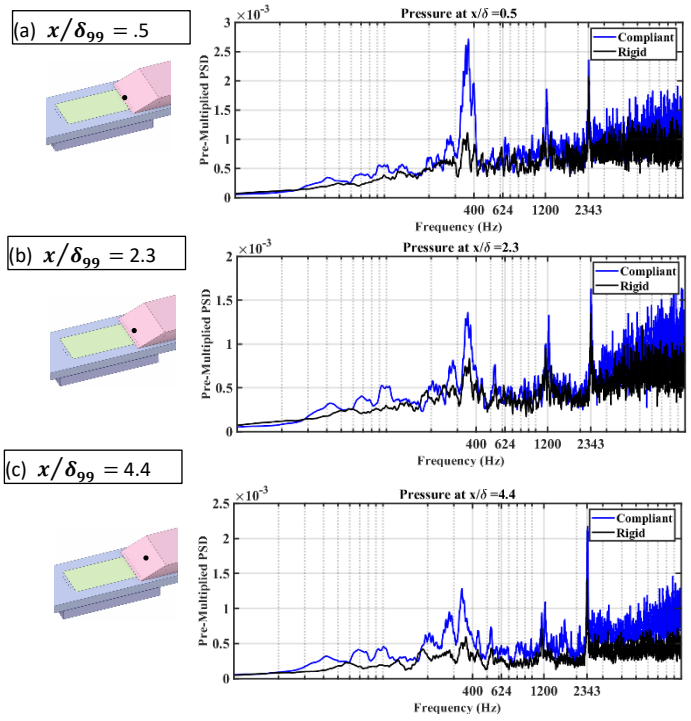

Figure 6. Premultiplied power spectral density of virtual pressure transducer data on the ramp face for rigid and compliant panels. (a) $x/\delta_{99} = 0.5$, (b) $x/\delta_{99} = 2.3$, and (c) $x/\delta_{99} = 4.4$

Downloaded by Noel Clemens on August 8, 2021 | http://arc.aiaa.org | DOI: 10.2514/6.2021-2809

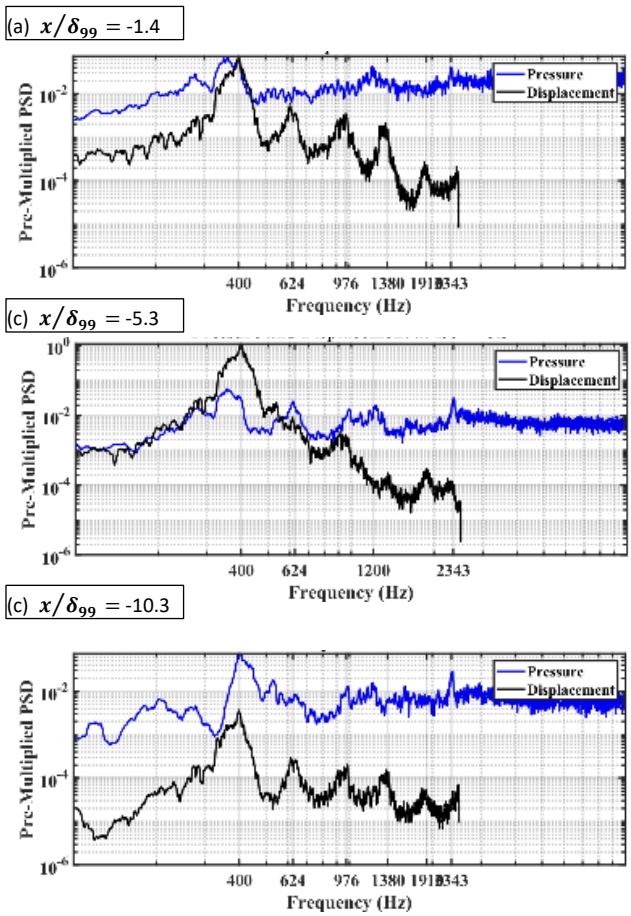

Figure 7. Premultiplied power spectral density of displacement and virtual pressure on the panel surface (a) x/δ_{99} = -1.4, (b) x/δ_{99} =-5.3, and (c) $x/\delta_{99} = -10.3$

H. Spectral Proper Orthogonal Decomposition Analysis

The spatial mode shapes associated with compliant panel vibratory response lend themselves to analysis using proper orthogonal decomposition (POD); however, the standard snapshot POD method does not use time-correlated data and so all spectral content is lost. In contrast, spectral proper orthogonal decomposition (SPOD) uses time-dependent flow realizations and thus retains dynamical information, making it a good candidate for analyzing FSI [24]. SPOD creates a series of mode shapes, each associated with a frequency band that can then be ranked by mode energy. Using SPOD allows us to examine the mode shapes of the panel displacement and structures within the SBLI pressure footprint while retaining spectral information.

The Matlab code written by Towne et al. [24] was used. SPOD allows the calculation of multiple modes, which can be ranked from the most to least energetic. Since the most energetic SPOD mode gives the peak value at 400Hz, which corresponds to the first panel mode and contains most of the total modal energy, we considered only the first SPOD mode to analyze. Figure 8 shows the first mode energy level of the SPOD for both the DIC and PSP as a function of frequency for the compliant panel case. Figure 8 shows peaks near the first panel vibration frequency (near 400 Hz) for both the displacement and pressure. This observation supports the concept that the first mode of the panel is important in coupling to the flow features. The other peaks on the displacement PSD shown in

Downloaded by Noel Clemens on August 8, 2021 | http://arc.aiaa.org | DOI: 10.2514/6.2021-2809

Figure 7(a,c) are also observed as local peaks in the SPOD (Figure 8), and so those peak values were considered to compare the mode shapes at those frequencies.

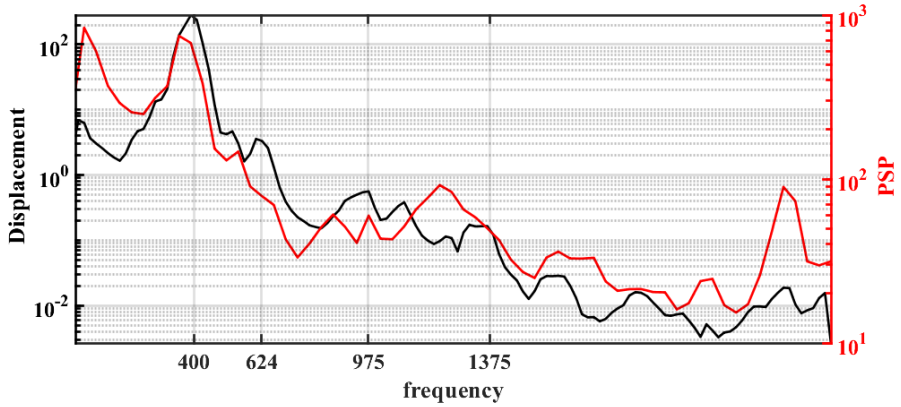

Figure 8. The first SPOD mode energy level of displacement and pressure

Figure 9 shows SPOD mode shapes of displacement and pressure at frequencies of 400, 624, 975 and 1374 Hz. The frequency at 1918 Hz was not considered since it was not present in both the displacement and pressure fields. Figure 9a shows the first mode shape at ~400Hz for pressure and displacement. The first-mode surface displacement shape introduces a gradient in the surface displacement (i.e., change in local flow angle) from the upstream edge of the plate until the intermittent region. This gradual change in flow angle causes a resultant change in the pressure field, and this effect can be quantified using linearized theory for supersonic potential flow [23]. Indeed, the SPOD mode shape shows the expected distribution of pressure for the first-mode displacement of the panel from $x/\delta_{99} \approx -10$ to the intermittent region $x/\delta_{99} \approx -2$. Figure 9(b) shows the second mode shape for displacement, and the displacement trend shows agreement with the pressure variation on the PSP. Additionally, the shock foot location on the panel is marked as a yellow line near $x/\delta_{99} \approx -2.5$. The third and fourth mode shapes of displacement were calculated at frequencies at 975 and 1375 (Figure 9c,d). Corresponding third and fourth mode shapes for displacement and pressure agree well.

Downloaded by Noel Clemens on August 8, 2021 | http://arc.aiaa.org | DOI: 10.2514/6.2021-2809

Downloaded by Noel Clemens on August 8, 2021 | http://arc.aiaa.org | DOI: 10.2514/6.2021-2809

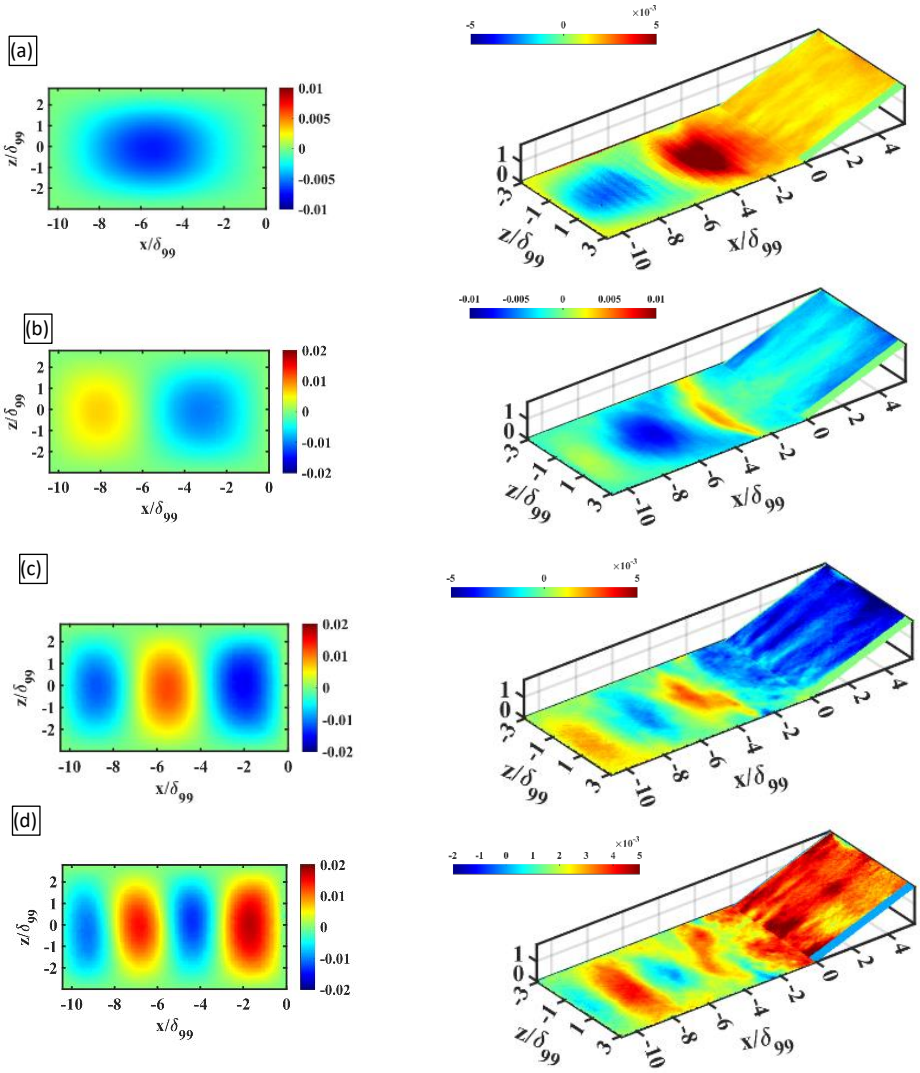

Figure 9. SPOD of displacement and pressure for the compliant panel. Left and right columns are for displacement and pressure, respectively. (a) *f =400* Hz, (b) *f =625* Hz, (c) *f* = 975 Hz, and (d) *f* = 1375 Hz.

I. Bandpass filtered data

The flow-structure coupling was further analyzed by bandpass filtering displacement and pressure data around the same modal frequencies identified in the previous section and using a bandwidth of 30 Hz. This analysis is similar to that conducted by Eitner [23] for analyzing aeroelastic coupling for brass panels with smaller displacement magnitudes. The current analysis was made for the entire pressure field in the current study, including the ramp face, and thus allows comparison to the SPOD results. Both deformation and displacement data were bandpass filtered using Matlab 4th order Butterworth filter function by centering the frequencies on the previous section where SPOD modes were calculated at chosen peak values. The most energetic first mode (f=400 Hz) image sequence for pressure is shown in Figure 10. The time stamp is shown at the top of the images. The band-passed image sequence shows the presence of two prominent features: the first seems to be related to the shock foot near $x/\delta_{99} \approx -2$ and

the second are the low and high pressure regions that were previously attributed to the aerodynamic response to the panel curvature over the range $x/\delta_{99} \approx -10$ to -2.

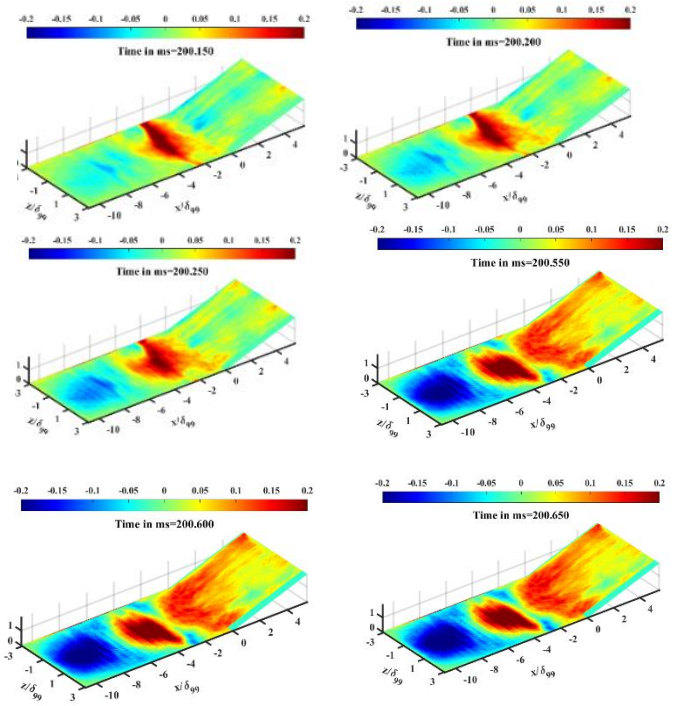

Figure 10 Time sequence images from bandpass filtered pressure field centered at *f*≈*395* Hz.

The bandpass-filtered pressure and displacement time-series data were further analyzed by conditionally-averaging all images for which the peak displacement values occur. The conditionally-averaged pressure and displacement fields, shown in Figure 11, should reflect the pressure field response when maximum forcing (i.e., highest displacement) occurs. Figure 11 shows similar displacement mode shapes as were observed using SPOD (Figure 9). The conditionally-average pressure field for the first mode (near 400 Hz) does not appear to show the intermittent region, which suggests the shock-foot motion is less correlated with the panel vibratory response. This observation of the shock foot seems to be in disagreement with previous studies that showed a stronger coupling of the shock foot motion to the panel vibration [11], [12], [23]. This apparent discrepancy will be a topic of future

Downloaded by Noel Clemens on August 8, 2021 | http://arc.aiaa.org | DOI: 10.2514/6.2021-2809

esearch. Figure 11 further shows that the higher mode shapes are quite similar to the previously-presented SPOD modes.

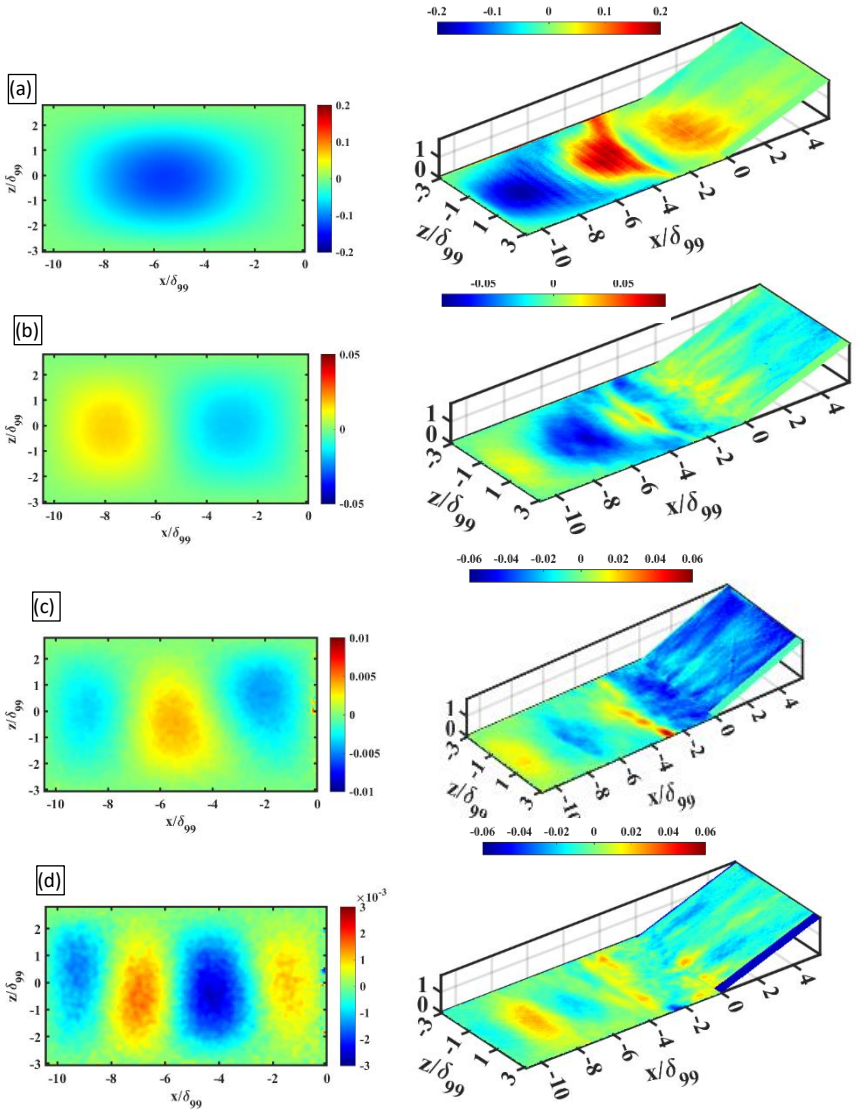

Figure 11. Conditionally-averaged displacement and pressure fields for peak displacement based on the band-pass filtered data. The left and right columns are for displacement and pressure, respectively. (a) *f* =*400*Hz, (b) *f* =*625* Hz, (c) *f* = 975 Hz, and (e) *f* = 1375 Hz.

III. Summary and Conclusions

The analysis of rigid and compliant panels under a compression-ramp SBLI was conducted using high-speed PSP and DIC. A unique aspect of this work is that the pressure field was measured on the rigid ramp face. This work focused on a single compliant panel case – 1 mm thick polycarbonate – since this case gave the largest displacement amplitudes without failure of the panel. The data were analyzed using standard spectral analysis, spectral proper

Downloaded by Noel Clemens on August 8, 2021 | http://arc.aiaa.org | DOI: 10.2514/6.2021-2809

orthogonal decomposition, bandpass filtering, and conditional averaging. The results reveal that, over most of the panel, there is a clear coupling of the pressure field to the panel vibratory response, which is consistent with linearized theory for supersonic potential flow. Further, the effect of the panel displacement can be observed well onto the ramp face, although this effect diminishes with downstream distance. This observation indicates that the shear layer reattachment process is coupled with the panel vibration. The shock foot does not seem to be as strongly correlated to the panel displacement, especially the first mode, which seems to be in disagreement with previous work. It was also observed that the SPOD and bandpass filtered data agree well on the nature of the mode shapes inferred from the displacement and pressure data.

References

[1] J. J. McNamara and P. P. Friedmann, "Aeroelastic and Aerothermoelastic Analysis in Hypersonic Flow: Past, Present, and Future," *AIAA J.*, vol. 49, no. 6, pp. 1089–1122, 2011, doi: 10.2514/1.J050882.

[2] D. S. Dolling, "Fifty Years of Shock-Wave/Boundary-Layer Interaction Research: What Next?," *AIAA J.*, vol. 39, no. 8, pp. 1517–1531, Aug. 2001, doi: 10.2514/2.1476.

[3] N. T. Clemens and V. Narayanaswamy, "Low-Frequency Unsteadiness of Shock Wave/Turbulent Boundary Layer Interactions," *Annu. Rev. Fluid Mech.*, vol. 46, no. 1, pp. 469–492, Jan. 2014, doi: 10.1146/annurev-fluid-010313-141346.

[4] H. Babinsky and J. K. Harvey, *Shock Wave-Boundary-Layer Interactions*. Cambridge: Cambridge University Press, 2011.

[5] S. Willems, A. Gülhan, and B. Esser, "Shock induced fluid-structure interaction on a flexible wall in supersonic turbulent flow," Progress in Flight Physics 5, vol. 5, pp. 285–308, 2013, doi: 10.1051/eucass/201305285.

[6] L. Maestrello and T. L. J. Linden, "Measurements of the response of a panel excited by shock boundary-layer interaction," *J. Sound Vib.*, vol. 16, no. 3, pp. 385–388, 1971, doi: 10.1016/0022-460X(71)90594-3.

[7] S. M. Spottswood, T. Eason, and T. Beberniss, "Full-field, dynamic pressure and displacement measurements of a panel excited by shock boundary-layer interaction," May 2013, doi: 10.2514/6.2013-2016.

[8] S. M. Spottswood *et al.*, "Exploring the response of a thin, flexible panel to shock-turbulent boundary-layer interactions," *J. Sound Vib.*, vol. 443, pp. 74–89, 2019, doi: 10.1016/j.jsv.2018.11.035.

[9] S. M. Spottswood, T. Eason, and T. Beberniss, "Influence of shock-boundary layer interactions on the dynamic response of a flexible panel," *Proc. Int. Conf. Noise Vib. Eng. ISMA 2012*, pp. 603–616, 2012.

[10] M. Eitner, M. Musta, L. Vanstone, J. Sirohi, and N. Clemens, "Modal Parameter Estimation of a Compliant Panel Using Phase-based Motion Magnification and Stereoscopic Digital Image Correlation," *Exp. Tech.*, pp. 287–296, 2020, doi: 10.1007/s40799-020-00393-6.

[11] T. J. Goller, D. U. Mustafa N. Musta, Leon Vanstone, and N. T. C. Lee Mears, Jayant Sirohi, "Simultaneous High-Speed Displacement and Surface Pressure Measurements of a Compliant Panel under a Mach 2 Compression Ramp Interaction,", *Presented in AIAA SciTech Invited Session*, 2019.

[12] T. J. Goller, M. N. Musta, D. Uehara, & Sirohi, J., and N. Clemens, "Experimental Study of a Compliant Panel under a Mach 2 Compression Ramp Interaction," *71st Annual Meeting of the APS Division of Fluid Dynamics,* 2018.

Downloaded by Noel Clemens on August 8, 2021 | http://arc.aiaa.org | DOI: 10.2514/6.2021-2809

[13] M. Musta, L. Vanstone, M. Eitner, J. Sirohi, and N. T. Clemens, "A Compression - Ramp Shock/Boundary-Layer Interaction Over a Compliant Panel at Mach 5," *72nd Annual Meeting of the APS Division of Fluid Dynamics*,2019.

[14] T. J. Goller, "Simultaneous High-Speed Displacement and Surface Pressure Measurements of a Compliant Panel under a Mach 2 Compression Ramp Interaction," MSc. Thesis, the University of Texas at Austin, 2019.

[15] Y. Hou, "Particle image velocimetry study of shock-induced turbulent boundary layer separation," 2003, [Online]. Available: http://www.lib.utexas.edu/etd/d/2003/houy039/houy039.pdf.

[16] B. Ganapathisubramani, "Statistical properties of streamwise velocity in a supersonic turbulent boundary layer," *Phys. Fluids*, vol. 19, no. 9, p. 098108, 2007, doi: 10.1063/1.2772303.

[17] L. Vanstone, M. N. Musta, S. Seckin, and N. Clemens, "Experimental study of the mean structure and quasi-conical scaling of a swept-compression-ramp interaction at Mach 2," *J. Fluid Mech.*, vol. 841, pp. 1–27, Apr. 2018, doi: 10.1017/jfm.2018.8.

[18] R. D. Blevins and R. Plunkett, *Formulas for Natural Frequency and Mode Shape*, vol. 47, no. 2. New York: Van Nostrand Reinhold Co., 2009.

[19] A. J. Wheeler and A. R. Ganji, *Introduction to Engineering Experimentation*, 2nd ed. New Jersey, New York: Prentice-Hall, 1996.

[20] Y. Egami, Y. Hasegawa, Y. Matsuda, T. Ikami, and H. Nagai, "Ruthenium-based fast-responding pressure-sensitive paint for measuring small pressure fluctuation in low-speed flow field," *Meas. Sci. Technol*., vol. 32, no. 2, 2021, doi: 10.1088/1361-6501/abb916.

[21] M. Eitner, M. Musta, L. Vanstone, J. Sirohi, and N. Clemens, "Modal Parameter Estimation of a Compliant Panel Using Phase-based Motion Magnification and Stereoscopic Digital Image Correlation," *Exp. Tech.*, 2020, DOI: 10.1007/s40799-020-00393-6.

[22] L. Vanstone and N. T. Clemens, "Unsteadiness Mechanisms of a Swept Compression-Ramp Shock / Boundary Layer Interaction at Mach 2," *AIAA Scitech 2019 Forum*, no. January, pp. 1–19, 2019, doi: 10.2514/6.2019-0095.

[23] M. A. Eitner, "Experimental Investigation of Fluid-Structure Interaction of a Compliant Panel under a Mach 2 Compression Ramp Shock-Boundary Layer Interaction," Ph.D. Thesis, the University of Texas at Austin, 2021.

[24] A. Towne, O. T. Schmidt, and T. Colonius, "Spectral proper orthogonal decomposition and its relationship to dynamic mode decomposition and resolvent analysis," *J. Fluid Mech.*, vol. 847, pp. 821–867, 2018, doi: 10.1017/jfm.2018.283.

Downloaded by Noel Clemens on August 8, 2021 | http://arc.aiaa.org | DOI: 10.2514/6.2021-2809